Journal of Power Sources 185 (2008) 1305–1310

Contents lists available at ScienceDirect

Journal of Power Sources

journal homepage: www.elsevier.com/locate/jpowsour

Short communication

Integrated micro-power source based on a micro-silicon fuel cell and a micro electromechanical system hydrogen generator

L. Zhu [a,*], K.Y. Lin [b], R.D. Morgan [b], Vikhram V. Swaminathan [a], H.S. Kim [b], B. Gurau [b], D. Kim [c], B. Bae [a,d], R.I. Masel [b,d], M.A. Shannon [a,b,d]

[a] Department of Mechanical Science and Engineering, University of Illinois at Urbana Champaign, 1206 West Green Street, Urbana, IL 61801, USA
[b] Department of Chemical and Biomolecular Engineering, University of Illinois at Urbana Champaign, 600 South Mathews Avenue, Urbana, IL 61801, USA
[c] Department of Mechanical Engineering, Sogang University, 1 Shinsu-dong, Mapo-gu, Seoul, Republic of Korea
[d] Cbana Labs, Inc. Champaign, IL, USA

ARTICLE INFO

Article history:
Received 14 August 2008
Accepted 10 September 2008
Available online 19 September 2008

Keywords:
Micro-power source
Micro-silicon fuel cell
Hydrogen generator
Self-regulating mechanism

ABSTRACT

Micro-power sources that are comparable to or smaller than the size of the micro-devices needing power are needed for many applications. This paper introduces an integrated millimeter scale power source based on a micro-silicon fuel cell and a MEMS hydrogen generator, with passive control. The integrated devices are fabricated from silicon wafers using conventional MEMS fabrication processes. In this design, the hydrolysis reaction of calcium hydride and water is used to generate hydrogen, and the hydrogen generation rate is controlled by a microfluidic self-regulating mechanism, which can control the hydrolysis reaction based on the load. Design, fabrication, and testing results of a prototype system are described. One of the devices can produce 90 μW for 6 h with a maximum power of 0.17 mW, and another one can produce 30 μW for 26 h with a total energy density of 100 Wh L^{-1}.

1. Introduction

There is a growing need for micro-power sources, which are comparable to the size of the micro-devices that they are powering, due to the fast growth of Micro Electromechanical System (MEMS) devices. For instance, sub-millimeter sized sources producing micro-watts of steady-state power with peaks to milli-watts are needed for many types of micro-sensors, cognitive arthropods, subdermal drug delivery systems, and other applications. Generally, the devices have mission durations of an hour to a few months. To this end, sub-millimeter power sources with such power and energy densities have not yet been demonstrated due to constraints on packaging, fuel storage, fuel delivery, and power generation. Most MEMS devices are still powered by external macroscopic power supplies, and in some cases, the large power supplies eliminate the advantages of the reduction in device size.

In order to solve this problem, many small power sources have been explored, such as biofuel cells [1–10], energy harvesting devices [11,12], ultra-capacitors [13,14], micro-batteries [15–24], etc. Typical millimeter sized biofuel cells and miniature energy harvesting devices produce peak powers of a few micro-watts or less, which is usually not sufficient for most applications. Ultra-capacitors produce high peak powers, but their energy density is low and usually less than 10 Wh kg^{-1}. Their main applications include boost components for supporting batteries and fuel cells. Micro-batteries have also been widely explored to build millimeter scale power sources and some efforts have been done to miniaturize the power sources to sub-millimeter scale. For instance, the all solid-state thin film lithium battery is a highly promising and mature system already under development by a number of entities with ties to the original work at Oakridge National Laboratory [15,17]. Although planar thin film micro-batteries have relatively high power per unit volume, the current density per unit area is low (1–10 mA cm^{-2}) due to the size of the surface area (centimeter scale). If the area of the thin film battery is decreased to the millimeter scale, the maximum power would be in the micro-watt range. Therefore, multiple thin film cells have to be stacked in the *z* direction to meet the peak power requirement. This process could cause challenging in fabrication and packaging, as well as increasing the internal resistance, which drops the power density nonlinearly. A 3-D integrated all-solid-state rechargeable micro-battery has been proposed [25], but this battery is still in the early stages of development.

Recently, micro-fuel cells have attracted lots of attention as millimeter scale power sources due to their inherently higher energy

* Corresponding author. Tel.: +1 217 244 7301; fax: +1 217 2446534.
E-mail address: lzhu@illinois.edu (L. Zhu).

0378-7753/$ – see front matter © 2008 Elsevier B.V. All rights reserved.
doi:10.1016/j.jpowsour.2008.09.028

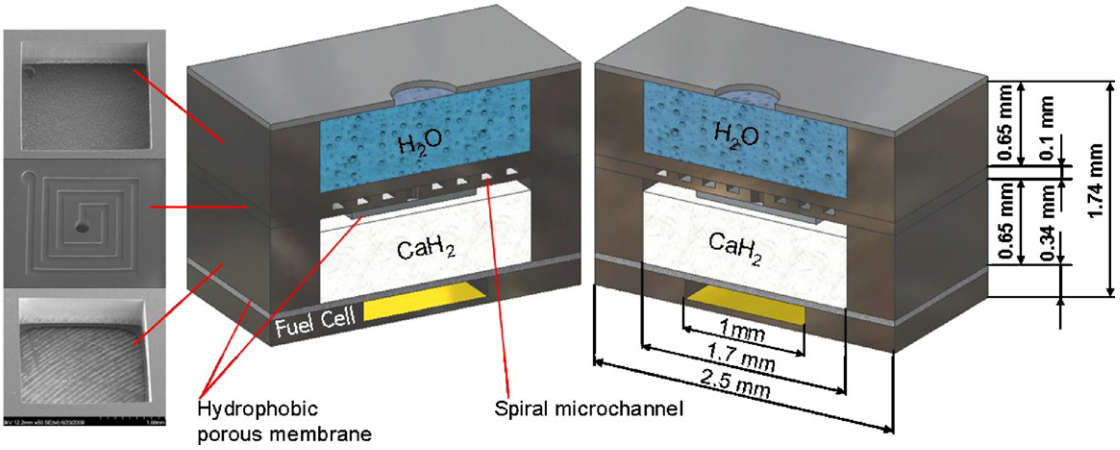

Fig. 1. Schematic of the all silicon integrated micro-power source based on self-regulating MEMS hydrogen generator and micro-silicon fuel cell. SEM images of the water chamber, control layer with spiral microchannel, and hydride chamber are shown on the left side of the schematic. The dimension of the device is 2.5 mm × 2.5 mm × 1.74 mm, and the whole volume of the device is 10.9 μL.

and power densities. Most of the current research work is focused on the development of portable proton exchange membrane (PEM) fuel cells that meet the demand of portable electronic devices with 1–10 W electric power [26–28]. Millimeter scale silicon fuel cells have been explored by several groups [29–32]. In a previous paper, we presented a micro-fuel cell integrated to a MEMS hydrogen generator, that produced a low output power [33]. In this paper, we present the design, fabrication, and initial testing results of an integrated micro-power source based on a micro-silicon fuel cell and a MEMS hydrogen generator with a different design than in our previous paper. This design produces much higher peak powers than our previous design.

This paper first presents the fabrication processes of the micro-silicon fuel cell, the MEMS hydrogen generator, and the integration process between the two components. The performance of the micro-power source is also presented and compared with the performance of the micro-fuel cell before integration. The mechanisms that limit the performance of the integrated micro-device are detailed, and the microfluidic self-regulating mechanism for controlling hydrogen generation from metal hydride is discussed. Finally lifetime test results of two fabricated devices are presented and discussed.

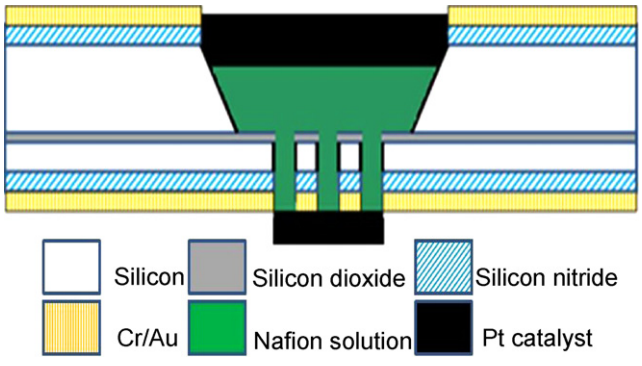

Fig. 2. Schematic of Si based hybrid membrane hydrogen fuel cell. The micro-silicon fuel cell dies are fabricated from a double-sided polished SOI wafer with a 300 μm thick handle wafer, 40 μm thick device layer and 0.5 μm thick buried oxide using conventional MEMS fabrication processes. Nafion® ionomer 1100 EW was applied to the membrane area to fill the channels for proton conduction. The platinum black catalyst inks were painted onto the Nafion® layer to form the membrane electrode assembly.

2. Experimental

The device schematic is shown in Fig. 1 and the volume of the whole device is 10.9 mm^3 (2.5 mm × 2.5 mm × 1.74 mm). Both the micro-silicon fuel cell and the MEMS hydrogen generator are fabricated from silicon wafers using standard MEMS fabrication processes, which enable the miniaturization of the micro-system down to a sub-millimeter power source. In this work, calcium hydride (CaH_2) is used as the fuel due to its high energy density, fast and complete reaction, and low volume expansion [34]. CaH_2 is not typically used for large scale mobile hydrogen generators due to its higher weight per hydrogen stored, but for the device described here, small volumes are more important than low weight. As shown in Fig. 1, a microfluidic self-regulating mechanism is integrated into the MEMS hydrogen generator to control the hydrogen generation based on the load. The self-regulating mechanism is fully passive and does not cause any parasitic power loss. The current work investigates a feasible approach to a fully functioning sub-millimeter power source in the future.

2.1. Microfabrication of micro-silicon fuel cell dies

The micro-silicon fuel cell depicted in Fig. 2 is fabricated from a 100 mm P type boron-doped double-sided polished prime ⟨1-0-0⟩ SOI wafer (Ultrasil Corp., Hayward, CA) with a 300 μm thick handle wafer (0.1–1.0 Ω cm resistivity), 40 μm thick device layer (1–10 Ω cm resistivity), and 0.5 μm thick buried oxide using conventional MEMS fabrication processes. Square windows of 2.4 mm × 2.4 mm were patterned on the handle wafer (anode side) while a 6 × 6 array of circular windows of 100 μm diameter and 100 μm apart were patterned on the device layer (cathode side). Fig. 3 shows the microfabrication process for the Si dies: (A) The native oxide layer was removed by immersion in buffered oxide etch (BOE) solution and the wafer was cleaned using piranha etch (3:1 sulfuric acid and 30 wt% hydrogen peroxide); (B) approximately 100 nm thick silicon nitride layer was grown on both sides of the wafer by low pressure chemical vapor deposition (LPCVD); (C) AZ 4620 photoresist (Clariant Co., Somerville, NJ) was used to pattern the silicon nitride of the handle wafer (anode side) to make the square windows (2.4 mm sides); (D) Dry etching using inductively coupled plasma-deep reactive ion etching (ICP-DRIE) was done to create square windows in the nitride layer on the anode side; (E) Photoresist was removed by photoresist stripper AZ-400T (Clariant

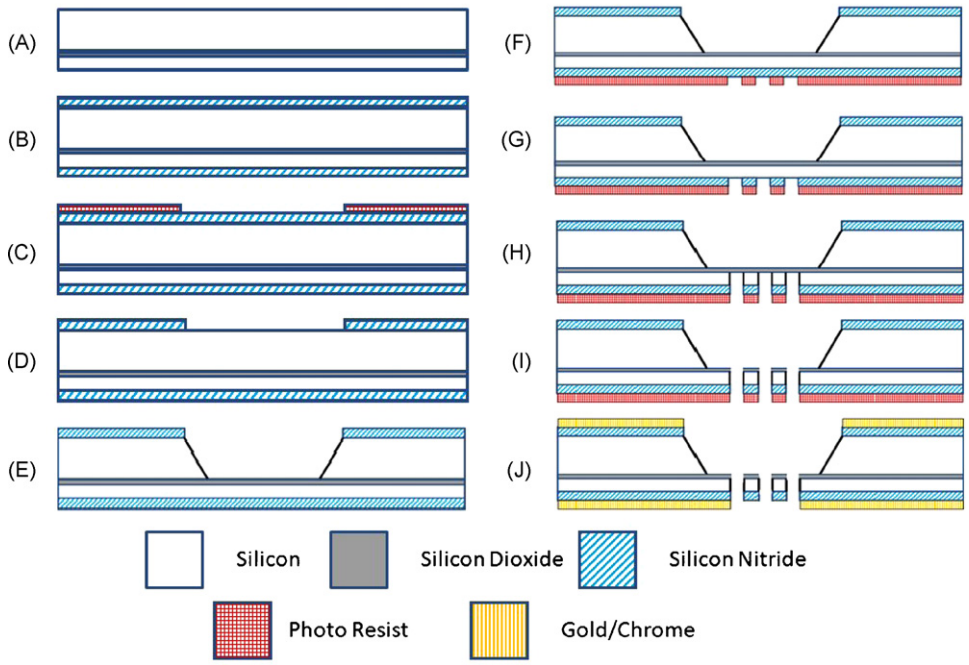

Fig. 3. Microfabrication processes for silicon fuel cell dies.

Co.), then the exposed silicon substrate was wet etched down to the oxide layer using a 35% potassium hydroxide (KOH) solution at 85 °C with silicon nitride as the mask; (F) Again, using standard photolithography, a 6 × 6 array of circular windows (100 μm diameter) was patterned on the silicon nitride of the device layer (cathode side); (G) Dry etching using ICP-DRIE was done to create the circular windows in the silicon nitride on the cathode side; (H) Dry etching using the BOSCH process was done to etch 40 μm of the exposed silicon substrate down to the oxide layer; (I) Dry etching using a Freon reactive ion etcher system (Freon RIE, PlasmaLab) was done to etch through the oxide layer; (J) Using a DC-Magnetron sputtering system, roughly 150 nm of gold with 50 nm of chrome as an adhesion layer was sputtered (on both sides of the wafer except the openings) to serve as the current collector. Fig. 4 shows the SEM images of the fabricated micro-silicon fuel cell dies.

2.2. Preparation of membrane electrode assembly

The membrane electrode assembly (MEA) was fabricated on the silicon structure as shown in Fig. 2. To prepare the MEA, ~28 μL of 5 wt.% Nafion® ionomer 1100 EW (Solution Technology Inc., Mendenhall, PA) was applied to the membrane area to fill the channels for proton conduction as well as to serve as an adhesion layer for the anode and cathode catalyst layers. The Nafion® layer was then allowed to dry. Catalyst inks were prepared by dispersing platinum black (HiSPEC 1000, Alfa Aesar, Ward Hill, MA) with Nafion® solution, Millipore water, and isopropanol via sonication. Using the direct paint method, the catalyst inks were painted onto the Nafion® layer of the anode and cathode to form the membrane electrode assembly. The resulting catalyst loading was approximately 20 mg cm^{-2}. In addition to the membrane area, a small amount of catalyst ink was painted onto the gold current collectors to provide electrical connection.

2.3. Microfabrication of MEMS hydrogen generator

As shown in Fig. 1, the MEMS hydrogen generator was fabricated from three silicon wafers. The water reservoir and hydride reservoir were fabricated from 650 μm thick, double side polished prime wafers using ICP-DRIE. The hydride reservoir is 1.7 mm × 1.7 mm × 0.65 mm and the water reservoir is 1.7 mm × 1.7 mm × 0.55 mm with a 200 μm through hole at the corner. The microfluidic self-regulating mechanism was fabricated from a 100 μm thick, double-sided polished prime wafer. A 100 μm wide, 30 μm deep, and 11.9 mm long spiral microchannel and a 200 μm diameter hole at center end of the spiral microchannel

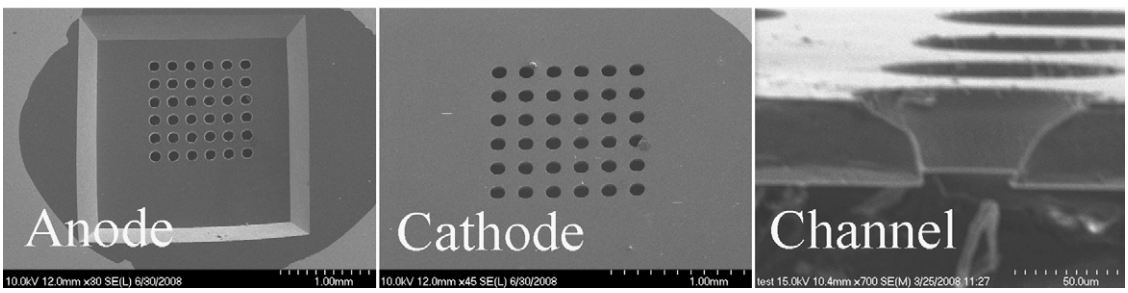

Fig. 4. SEM images showing fabricated micro-silicon fuel cell dies from cathode side and anode side views. Square windows of 2.4 mm × 2.4 mm were patterned on the handle wafer (anode side) while a 6 × 6 array of circular windows of 100 μm diameter and 100 μm apart were patterned on the device layer (cathode side).

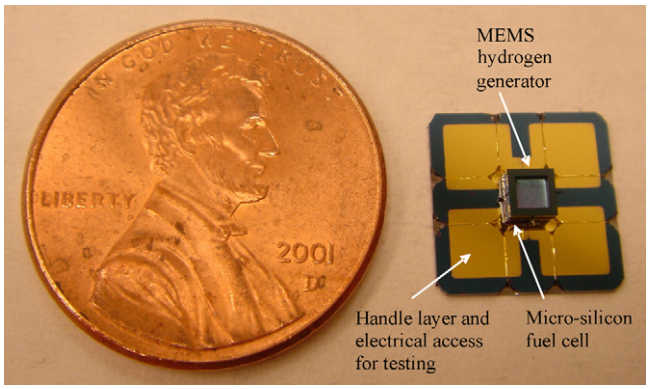

Fig. 5. Pictures of the MEMS hydrogen generator and integrated micro-power source with micro-silicon fuel cell.

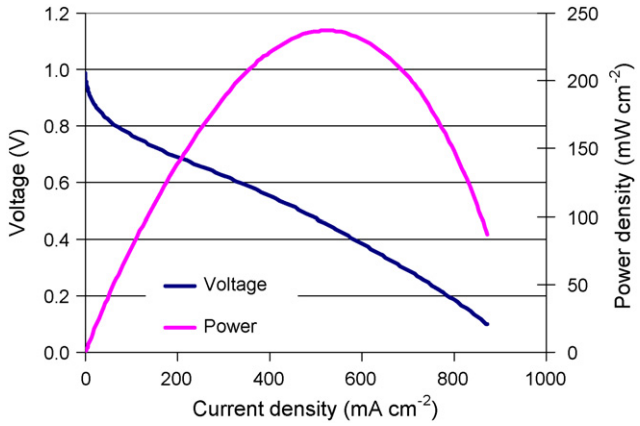

Fig. 7. Polarization curve and power density plot of the micro-silicon fuel cell before integration. This micro-silicon fuel cell has an open cell potential of 0.98 V and a peak power density of 237 mW cm^{-2}. Hydrogen was supplied from a hydrogen tank.

were fabricated on this wafer using ICP-DRIE. To make the surface of water reservoir and microchannel hydrophilic, 0.5 μm of silicon dioxide was grown on the surface in an 1100 °C oxidation tube furnace for 12 h. The water reservoir was aligned and bonded to the microfluidic control layer by adhesive bonding [35] to seal the microchannel and make fluidic connection. A 50 μm thick porous hydrophobic PTFE membrane (GE Osmonics Labstore, Minnetonka, MN) was bonded to the control layer to prevent liquid water flowing into the hydride reservoir through the microchannel. The hydride reservoir was then bonded to the stack (water reservoir and control layer) to complete the fabrication of the MEMS hydrogen generator. Finally, CaH_2 powder (Aldrich Chemical Company, St. Louis, MO) was loaded into the hydride reservoir in a nitrogen glove box, and the MEMS hydrogen generator was bonded to the micro-fuel cell separated by a porous PTFE membrane. A photograph of a fabricated device using this approach is shown in Fig. 5.

2.4. Fuel cell testing

The micro-silicon fuel cell was tested using a potentiostat (Solartron SI 1287, Solartron Analytical, Hampshire, UK). In order to compare the fuel cell performance before and after integration, the fuel cell was tested before integration in a Teflon holder, which was fabricated in house as shown in Fig. 6. The Teflon holder consisted of two pieces. The bottom piece allowed hydrogen to flow over the anode, while the top piece allowed quiescent air to diffuse to the cathode. The fuel cell was placed in the Teflon housing and connected to the potentiostat. Dry hydrogen from a hydrogen tank was passed over to the anode with a flow rate of 1 sccm, and oxygen was allowed to diffuse to the cathode from ambient air. Once the fuel cell reached a steady open cell voltage (OCV), the potential was then stepped from the open cell voltage to 0.1 V and the current was recorded at each step.

3. Results and discussion

Fig. 7 shows the polarization curve and current density plot of a micro-silicon fuel cell before integration. The fuel cell testing set-up shown in Fig. 6 was used for this testing. The hydrogen is from a hydrogen tank, and the oxygen is from the ambient air. This micro-silicon fuel cell has an open cell potential (the voltage output of the fuel cell in the zero current density limit) of 0.98 V and a peak power density of 237 mW cm^{-2} (0.46 V, 520 mA cm^{-2}).

Two prototype devices were fabricated to evaluate the performance of the integrated micro-power source. A hydrogen purging system was built and the device was purged with hydrogen for three cycles to replace trapped nitrogen with hydrogen. The water

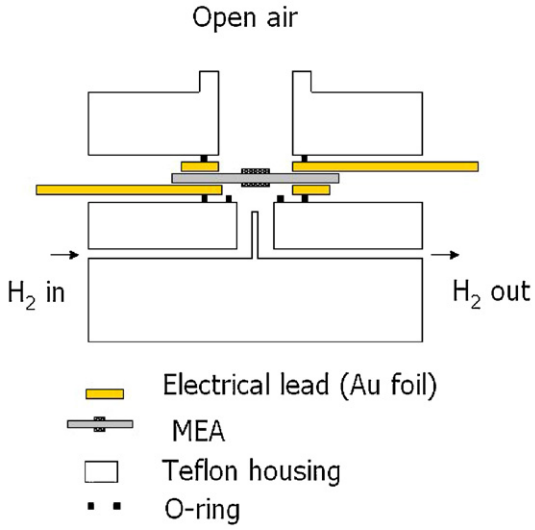

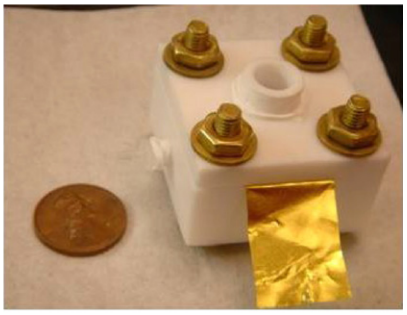

Fig. 6. Teflon housing for silicon fuel cell testing. The Teflon holder consisted of two pieces. The bottom piece allowed hydrogen to flow over the anode, while the top piece allowed quiescent air to diffuse to the cathode.

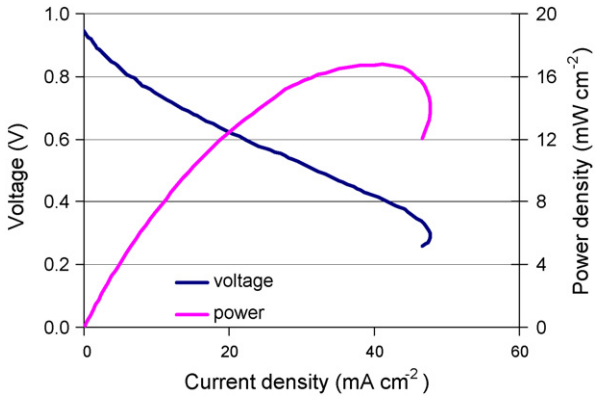

Fig. 8. Polarization curve and power density plot of the integrated device. Mass transfer limit was reached at 0.3 V due to the limited hydrogen generation rate.

reservoir was filled with Millipore water and sealed by Parafilm. The device was operated by vapor diffusion. Water flows from the water reservoir into the hydrophilic micro-channel where the water was in contact with the porous hydrophobic membrane. Water vapor diffuses through the membrane and spontaneously reacts with CaH_2 to release hydrogen ($CaH_2 + 2H_2O \rightarrow Ca(OH)_2 + 2H_2$). The hydrogen then flows to the anode of the fuel cell. The cathode of the fuel cell is exposed to ambient air to breath oxygen. The polarization curve and power density plot of one of the integrated micro-power sources are shown in Fig. 8. The device has an open cell potential of 0.95 V and a peak power density of 16.8 mW cm^{-2} (0.41 V, 41.1 mA cm^{-2}). The mass transport limit was reached at 0.3 V with current density of 48 mA cm^{-2}.

Chemical hydrides have been used to generate hydrogen for fuel cell applications for decades [36–38]. In this design, hydrogen production from CaH_2 is controlled by a microfluidic self-regulating mechanism. As shown in Fig. 9, water flows from the water reservoir into the hydrophilic microchannel and a hydrophobic porous membrane can prevent liquid water flowing into the hydride reservoir. Instead, the water vapor diffuses into the hydride reservoir through the hydrophobic porous membrane and reacts with the hydride to generate hydrogen. When hydrogen is being consumed at a low rate at the anode under a low load, the water-gas interface is forced to move back to the water reservoir. Therefore, the hydrogen generation rate decreases due to the longer water vapor diffusion length. As hydrogen is consumed by the fuel cell during periods

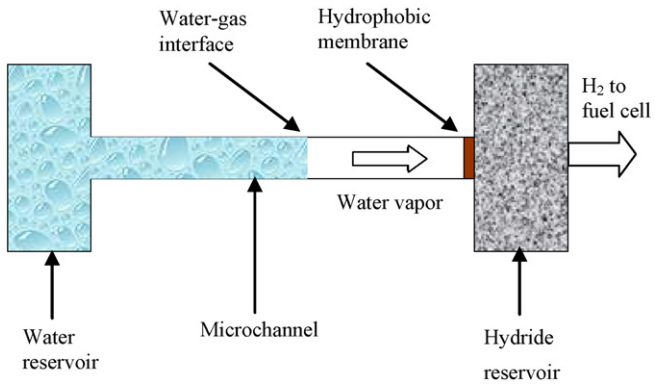

Fig. 9. Schematic of the microfluidic self-regulating mechanism for controlling hydrogen generation. Water flows from the water reservoir into the hydrophilic microchannel and a hydrophobic porous membrane can prevent liquid water flowing into the hydride reservoir. Water vapor diffuses into the hydride reservoir through the hydrophobic porous membrane and reacts with the hydride to generate hydrogen.

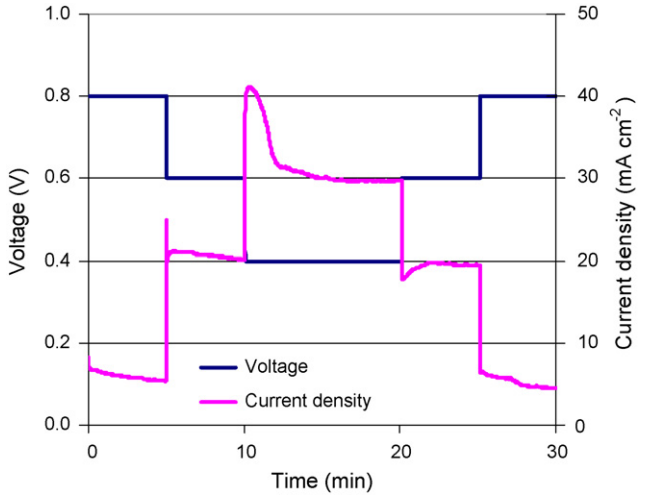

Fig. 10. Current density curve of the integrated device at 0.8, 0.6, and 0.4 V alternatively. The device was operated at each voltage for 5 min.

of load, the water–gas interface self-regulates to generate only the required amount of hydrogen. However, this self-regulating mechanism has both minimum and maximum hydrogen generation rates, when the water-gas interface is at the two ends of the microchannel, respectively. The integrated device was operated at 0.8, 0.6, and 0.4 V alternatively to test the self-regulating mechanism. Fig. 10 shows the current density plot of the integrated device at each voltage. Although the current density can quickly change when the voltage was changed, it stabilizes in about 5 min. This data indicates that the self-regulating mechanism can regulate the hydrogen generation with the load.

Lifetime tests were also performed at constant voltage (0.6 V) with the two fabricated devices. As shown in Fig. 11, one of the devices ran at 0.6 V for more than 6 h until the reaction was complete. Another device ran at 0.6 V with lower current density for more than 26 h. A summary of the testing results for the two devices is provided in Table 1. Device 1 has power density of 15.6 W L^{-1}, which is equal to an average power of 0.17 mW. Device 2 showed an energy density of 100 Wh L^{-1}, which is close to the energy density of current microbatteries [17]. The energy density can be improved if the fuel volume to device volume ratio (32% for current device) and fuel utilization rate (about 35% for current device) can be increased. Thinner fuel cell, control layer, and chamber walls can be fabricated in the next generation design to increase the fuel volume to device volume ratio and the energy density.

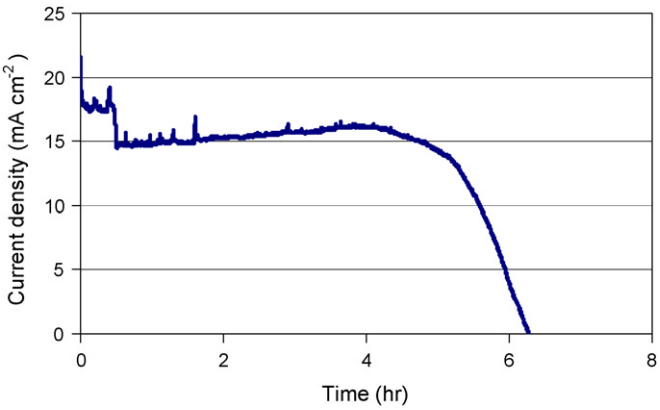

Fig. 11. Lifetime test for the integrated micro-power source. The micro-fuel cell was running at constant voltage 0.6 V for more than 6 h, and the total energy density (based on the volume of the whole device) is 61.3 Wh L^{-1}.

Table 1
Summary of the testing results for two fabricated devices based on micro-silicon fuel cell and MEMS hydrogen generator.

	Device volume (mm^3)	Open cell potential (V)	Energy density ($Wh\,L^{-1}$)	Maximum power density ($W\,L^{-1}$)
Device 1	10.9	0.99	61.3	15.6
Device 2	10.9	1.01	99.9	5.1

Compared with the fuel cell performance before integration shown in Fig. 6, the performance of the integrated device is about one order of magnitude lower. This reduction in power is because the Nafion® membrane was dehydrated by the strongly hygroscopic calcium hydride powder that is located on top of the Nafion® membrane. Most of the water in the Nafion® membrane from ambient air or from the cathode reaction can permeate through the membrane and react with the calcium hydride to release hydrogen. However, the proton conductivity of Nafion® is related to the water content within it [39]. Low water concentration in Nafion® can result in low fuel cell performance. On the other hand, the hydrogen generation rate is not high enough to produce high current. Several design approaches can be used to solve this problem. For instance, the water vapor can be delivered to the hydride by passing through the anode of the fuel cell, then the Nafion cannot be dehydrated. Another approach is to decrease the water vapor permeation rate from Nafion to the hydride by increasing the diffusion channel length or decreasing the cross-section area of the diffusion channel. The port on the microfluidic control layer separating liquid water and hydride water can be increased to get higher water vapor diffusion rate and higher hydrogen generation rate.

4. Conclusions

An integrated micro-power source based on a micro-silicon fuel cell and a MEMS hydrogen generator has been demonstrated in this paper. Two integrated devices were fabricated using MEMS fabrication processes. A microfluidic self-regulating mechanism has been successfully integrated into the micro-system, and this mechanism can control the hydrogen generation with changes in the applied electrical load. The performance of the integrated device is one order of magnitude lower than the micro-silicon fuel cell before integration due to the drying out of the Nafion® membrane by the hygroscopic calcium hydride in contact with it. One of the devices still has energy density of $100\,Wh\,L^{-1}$, which is close to the energy density of current microbatteries. The performance is expected to be improved in future designs that mitigate the dryout of the Nafion®.

Acknowledgements

This research is funded by the Defense Advanced Research Projects Agency (DARPA) under grant 2007-0299513-000. Any opinions, findings, and conclusions or recommendations expressed in this manuscript are those of the authors and do not necessarily reflect the views of the US Government. Micro-Nano-Mechanical Systems Cleanroom along with Micro and Nanotechnology Laboratory in University of Illinois at Urbana-Champaign provided the microfabrication facilities.

References

[1] R.A. Bullen, T.C. Arnot, J.B. Lakeman, F.C. Walsh, Biosens. Bioelectron. 21 (2006) 2015–2045.
[2] W.E. Farneth, M.B. D'Amore, J. Electroanal. Chem. 581 (2005) 197–205.
[3] E. Granot, E. Katz, B. Basnar, I. Willner, Chem. Mater. 17 (2005) 4600–4609.
[4] C. Kang, H. Shin, A. Heller, Bioelectrochemistry 68 (2006) 22–26.
[5] K. Rabaey, W. Verstraete, Trends Biotechnol. 23 (2005) 291–298.
[6] S.H. Shin, Y.J. Choi, S.H. Na, S.H. Jung, S. Kim, Bull. Korean Chem. Soc. 27 (2006) 281–285.
[7] S. Topcagic, S.D. Minteer, Electrochim. Acta 51 (2006) 2168–2172.
[8] M.K. Wang, F. Zhao, Y. Liu, S.J. Dong, Biosens. Bioelectron. 21 (2005) 159–166.
[9] X.C. Zhang, A. Ranta, A. Halme, Biosens. Bioelectron. 21 (2006) 2052–2057.
[10] Z.W. Zhu, C. Momeu, M. Zakhartsev, U. Schwaneberg, Biosens. Bioelectron. 21 (2006) 2046–2051.
[11] H.B. Fang, J.Q. Liu, Z.Y. Xu, L. Dong, D. Chen, B.C. Cai, Y. Liu, Chin. Phys. Lett. 23 (2006) 732–734.
[12] P. Singh, S. Kaneria, V.S. Anugonda, H.M. Chen, X.Q. Wang, D.E. Reisner, R.M. LaFollette, IEEE Sens. J. 6 (2006) 211–222.
[13] I.H. Kim, J.H. Kim, Y.H. Lee, K.B. Kim, J. Electrochem. Soc. 152 (2005) A2170–A2178.
[14] R. Kotz, M. Carlen, Electrochim. Acta 45 (2000) 2483–2498.
[15] J.B. Bates, N.J. Dudney, B. Neudecker, A. Ueda, C.D. Evans, Solid State Ionics 135 (2000) 33–45.
[16] A.M. Cardenas-Valencia, V.R. Challa, D. Fries, L. Langebrake, R.F. Benson, S. Bhansali, Sens. Actuators, B 95 (2003) 406–413.
[17] N.J. Dudney, Mater. Sci. Eng. 116 (2005) 245–249.
[18] A. Eftekhari, J. Power Sources 132 (2004) 240–243.
[19] D. Golodnitsky, V. Yufit, M. Nathan, I. Shechtman, T. Ripenbein, E. Strauss, S. Menkin, E. Peled, J. Power Sources 153 (2006) 281–287.
[20] S.W. Jeon, J.K. Lim, S.H. Lim, S.M. Lee, Electrochim. Acta 51 (2005) 268–273.
[21] K.L. Lee, J.Y. Jung, S.W. Lee, H.S. Moon, J.W. Park, J. Power Sources 129 (2004) 270–274.
[22] M. Nathan, D. Golodnitsky, V. Yufit, E. Strauss, T. Ripenbein, I. Shechtman, S. Menkin, E. Peled, J. Microelectromech. Syst. 14 (2005) 879–885.
[23] Y.H. Rho, K. Kanamura, J. Electroanal. Chem. 559 (2003) 69–75.
[24] C.L. Wang, L. Taherabadi, G.Y. Jia, M. Madou, Y.T. Yeh, B. Dunn, Electrochem. Solid-State Lett. 7 (2004) A435–A438.
[25] P.H.L. Notten, F. Roozeboom, R.A.H. Niessen, L. Baggetto, Adv. Mater. 19 (2007) 4564–4567.
[26] J.D. Morse, Int. J. Energy Res. 31 (2007) 576–602.
[27] K. Cowey, K.J. Green, G.O. Mepsted, R. Reeve, Curr. Opin. Solid State Mater. Sci. 8 (2004) 367–371.
[28] O.J. Adlhart, P. Rohonyi, D. Modroukas, J. Driller, Asaio J. 43 (1997) 214–219.
[29] T. Pichonat, B. Gauthier-Manuel, Fuel Cells 6 (2006) 323–325.
[30] K.L. Chu, M.A. Shannon, R.I. Masel, J. Electrochem. Soc. 153 (2006) A1562–A1567.
[31] K.L. Chu, S. Gold, V. Subramanian, C. Lu, M.A. Shannon, R.I. Masel, J. Microelectromech. Syst. 15 (2006) 671–677.
[32] K.L. Chu, M.A. Shannon, R.I. Masel, J. Micromech. Microeng. 17 (2007) S243–S249.
[33] S. Moghaddam, E. Pengwang, R.I. Masel, M.A. Shannon, J. Power Sources 185 (2008) 445–450.
[34] L. Zhu, D. Kim, H.S. Kim, R.I. Masel, M.A. Shannon, J. Power Sources 185 (2008) 1334–1339.
[35] B.R. Flachsbart, K. Wong, J.M. Iannacone, E.N. Abante, R.L. Vlach, P.A. Rauchfuss, P.W. Bohn, J.V. Sweedler, M.A. Shannon, Lab Chip 6 (2006) 667–674.
[36] Z.T. Xia, S.H. Chan, J. Power Sources 152 (2005) 46–49.
[37] D. Linden, Handbook of Batteries and Fuel Cells, McGraw-Hill Inc., New York, 1984.
[38] P.P. Prosini, P. Gislon, J. Power Sources 161 (2006) 290–293.
[39] R. O'Hayre, S.W. Cha, W. Colella, F.B. Prinz, Fuel Cell Fundamentals, John Wiley & Sons, Hoboken, NJ, 2006.